Vision, Modeling, and Visualization (2011)
Peter Eisert, Konrad Polthier, and Joachim Hornegger (Eds.)

Koiter's Thin Shells on Catmull–Clark Limit Surfaces

Anna Wawrzinek Klaus Hildebrandt Konrad Polthier

Freie Universität Berlin

Abstract

We present a discretization of Koiter's model of elastic thin shells based on a finite element that employs limit surfaces of Catmull–Clark's subdivision scheme. The discretization can directly be applied to control grids of Catmull–Clark subdivision surfaces, and, therefore, integrates modeling of Catmull–Clark subdivision surfaces with analysis and optimization of elastic thin shells. To test the discretization, we apply it to standard examples for physical simulation of thin shells and compute free vibration modes of thin shells. Furthermore, we use the discrete shell model to set up a deformation-based modeling system for Catmull–Clark subdivision surfaces. This system integrates modeling of subdivision surfaces with deformation-based modeling and allows to switch back and forth between the two different approaches to modeling.

Categories and Subject Descriptors (according to ACM CCS): I.3.5 [Computer Graphics]: Computational Geometry and Object Modeling—Physically based modeling

1. Introduction

Geometric design and modeling has always been intimately linked to the physics of elastic rods, plates, shells, or bodies. For example, the archetype of spline curves, the draftman's spline, is a thin elastic wood beam that is anchored in place by lead weights. Nowadays, shape design processes require an interplay of CAD systems for modeling and editing as well as FEA systems for analysis and optimization. A resulting problem is that the two types of systems are based on different geometry representations. Therefore, geometries have to be converted back and forth between the representations, which is a laborious process that often is only semi-automatic and causes approximation errors, see [HCY05]. This motivates to design schemes for the analysis and optimization of shapes that directly operate on CAD type of geometry representations.

A recent trend in geometry processing are deformation-based modeling schemes [BPGK06, BS08], which use energies based on models of elastic shells or solids for surface modeling. Such schemes can describe modeling operations by few constraints, and, therefore, allow for simple user-interfaces. Deformation-based modeling has originally been designed to enable modeling of 3d-scanned objects, and, therefore, schemes are formulated for triangle meshes. In order to integrate deformation-based modeling with a CAD system or a modeling system for computer animation, deformation-based modeling needs to be adapted to geometry representations used in these systems.

1.1. Contributions

We present a discretization of Koiter's model of elastic thin shells based on limit surfaces of Catmull–Clark's subdivision scheme and test it on standard examples for physical simulation of thin shells. We use the discrete shell model to set up a deformation-based modeling system for Catmull–Clark subdivision surfaces. This system integrates modeling of subdivision surfaces with deformation-based modeling and allows to switch back and forth between the two different approaches to modeling. As a third application, we compute the free vibration modes of thin shells.

1.2. Related work

Subdivision surfaces are common for modeling, especially in computer animation. Catmull–Clark's subdivision scheme [CC78] was one of the first and is tightly linked to surface representations with B-splines: the limit surface of a regular patch is a tensor product bi-cubic B-spline. Since limit surfaces are defined for irregular patches as

DOI: 10.2312/PE/VMV/VMV11/113-120

well, Catmull–Clark's scheme provides a way to generalize tensor product bi-cubic B-spline surfaces to meshes with arbitrary topology. Catmull–Clark limit surfaces are C^2 up to a finite set of isolated points that is only C^1; Reif and Schröder [RS01] showed that the second derivatives of Catmull–Clark limit surfaces are square integrable, hence elements of the Sobolev space H^2. Stam [Sta98] developed an algorithm to directly evaluate Catmull–Clark limit surfaces without having to refine them previously.

Koiter's model [Koi66, Koi70] is an example of a model of elastic thin shells that is based on the Kirchhoff–Love assumptions [Kir52, Lov88]. Conforming finite element discretizations of such models of thin shells require elements whose second derivatives are square integrable. Subdivison surfaces allow for an elegant construction of such elements and Loop's subdivision scheme has been used to discretize a Kirchhoff–Love type of thin shell model by Cirac et al. [COS00, CO01, CSA*02]. Recently, a scheme for simulation of elastic bodies based on an extension of Catmull–Clark's subdivision scheme to volumetric solids has been proposed by Burkhart et al. [BHU10].

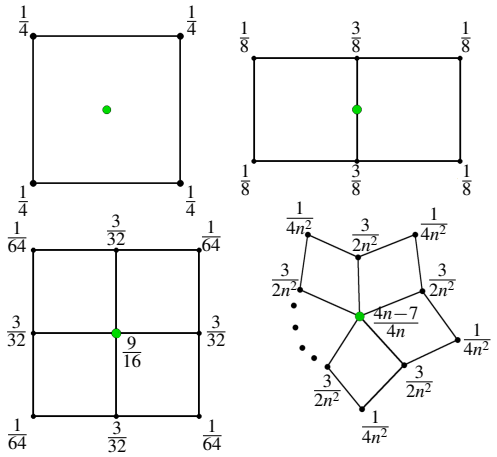

Figure 1: *Masks of the Catmull–Clark Subdivision for quadrangular meshes. The masks describes the weights of the corresponding vertices of the control grid used for the calculation of the new: element points, edge points and vertex points.*

2. Catmull–Clark Limit Surfaces

Subdivision schemes describe surfaces by an iterative refinement of a control grid. The repeated application of refinement rules generates in every subdivision step a new finer discrete surface. The series of grids converges towards a limit surface. Over the years, various subdivision schemes have been proposed. Refinement schemes are commonly specified by a subdivision mask, which specifies how to generate new vertices by averaging control vertices. For an overview of subdivision surfaces, we refer to [Ma05, PEK*08].

2.1. Catmull–Clark Subdivision Surfaces

The Catmull–Clark subdivision scheme [CC78] is designed for control grids with quadrilateral connectivity. On quad grids, we distinguish two types of elements: regular and irregular. An element is called regular if and only if all its vertices have valence four, where the valence of a vertex is the number of incident edges. For regular control grids the limit surfaces of Catmull–Clark's scheme are bi-cubic B-splines. Since Catmull–Clark surfaces are defined for irregular grids as well, they extend B-spline surface representations to control grids with arbitrary topology. Every iteration of Catmull–Clark's scheme produces three types of new vertices: element points, edge points and vertex points. Masks corresponding to the considered vertex type are illustrated in Figure 1.

2.2. Evaluation of Catmull–Clark Limit Surfaces

Stam [Sta98] introduced an algorithm to efficiently evaluate Catmull–Clark limit surfaces. In the following, we summarize this scheme, but we restrict our considerations to control grids whose irregular elements have only one vertex of valence unequal to 4, so called extraordinary elements. Note, that after one refinement step of Catmull–Clark's scheme all irregular elements of a quad grid are extraordinary. For every type of element the locations of control vertices in a prescribed stencil is considered (see Figure 2). The evaluation of the limit surface of every element type will be examined individually.

Regular elements

For a regular element, the limit surface corresponds to a uniform bi-cubic B-spline surface. We consider the control vertex matrix

$$C^T = (c_0, ..., c_{15})$$

where the columns c_i, $i = 0..., 15$, of this matrix are the coefficient vectors of the 16 vertices of the prescribed stencil. They correspond to the location of control vertices in a B-spline patch. The indices of the vertices are given in Figure 2. Furthermore, let $b(u,v)$ be the vector with the 16 bi-cubic B-spline base functions that are defined as follows:

$$b_i(u,v) := n_{i\%4}(u)\, n_{i/4}(v), \quad i = 0, ..., 15, \qquad (1)$$

where "%" and "/" describes the remainder and the division. The functions $n_j(t)$ are the four cubic B-spline basis func-

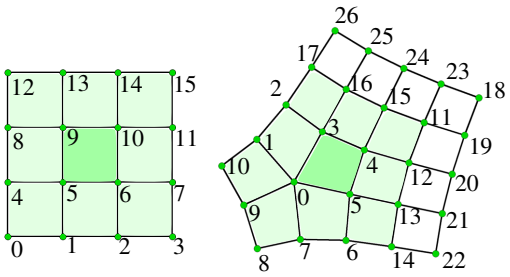

Figure 2: *Stencils for control vertex locations of a regular and irregular element where the irregular vertex have valence 5. Additionally, the indexing for the evaluation of the surface patches is given. The green colored areas describes the regular stencils of the elements. For the irregular element, the increase of the white colored elements represents the extended stencil, where stencils of three regular subelements can be considered.*

tions:

$$\begin{aligned} 6\,n_0(t) &:= (1-t)^3, \\ 6\,n_1(t) &:= 4-6t^2+3t^3, \\ 6\,n_2(t) &:= 1+3t+3t^2-3t^3, \\ 6\,n_3(t) &:= t^3 \end{aligned}$$

with $t \in [0,1]$. Then, the surface patch of a regular element is parametrized as

$$s(u,v) = C^T b(u,v), \quad (u,v) \in [0,1]^2. \tag{2}$$

The calculated patch is the limit surface of this element.

Irregular elements

Let us consider an extraordinary element with an irregular vertex of valence N. For the $K = 2N+8$ vertices of the initial stencil we specify a control vertex matrix

$$C_0^T = (c_0, \ldots, c_{K-1}),$$

where the indices of the corresponding vertices for $N = 5$ are given in Figure 2 (consider the green area of this stencil). For the subdivision of the associated stencil, two subdivision matrices are considered, the regular subdivision matrix A and the extended matrix $\bar{A}$. These determine two refined grids of the stencil. The coefficients of these matrices are listed in Figure 1. The difference between the subdivided grids is that, in the first case the structure of the refined mesh is identical to the initial stencil (see the green colored area in Figure 2). In the second case a refined mesh is given which contains regular stencils for one irregular and three regular subelements (see the green and white area in Figure 2).

Successive subdivision of an irregular element will produce a partition of the irregular element with a sequence of regular subelements. The control vertex matrix of the elements in the nth subdivision step is given by the relation

$$\bar{C}_n = \bar{A}C_{n-1} = \bar{A}A^{n-1}C_0, \quad n \geq 1, \tag{3}$$

where $C_{n-1} = A^{n-1}C_0$ describes the $(n-1)$th regular refinement step of the initial mesh. For the evaluation of the limit surface on the three regular subelements the vertices of the corresponding stencils are picked by a picking matrix P_k, $k = 1,2,3$, such that the control vertex matrix of the kth regular subelement for the nth subdivision step is given by

$$B_{k,n} = P_k \bar{C}_n, \quad k = 1,2,3,$$

where each row of P_k is filled with zeros except for a one in the column corresponding to the index in the stencil of this subelement. Then the surface patches of the regular subelements are

$$s_{k,n}(u,v) = B_{k,n}^T b(u,v) = C_0^T \left(P_k \bar{A} A^{n-1}\right)^T b(u,v), \tag{4}$$

for $(u,v) \in [0,1]^2$, where $b(u,v)$ denotes the bicubic B-spline basis functions (1). The functions

$$b_{k,n}(u,v) = \left(P_k \bar{A} A^{n-1}\right)^T b(u,v) \tag{5}$$

describe the basis functions of the corresponding regular subelement. The translation of the subelements to the corresponding domain of the partition provides the parametrization of the whole irregular element except the irregular vertex. This is given by

$$s(u,v)|_{\Omega_k^n} := s_{k,n}\left(t_{k,n}(u,v)\right), \tag{6}$$

where Ω_k^n is the domain of the kth regular subelement after the nth subdivision step. The function $t_{k,n}(u,v)$ describes the transformation of Ω_k^n onto the unit square. For details we refer to [Sta98].

3. Koiter's Thin Shells

We consider a homogeneous and isotropic thin shell whose undeformed shape is described by a middle surface with uniform thickness 2ε in normal direction. The shell can be parametrized by a system $\{x_1, x_2, x_3\}$ of curvilinear coordinates:

$$\Theta(x_1,x_2,x_3) := \theta(x_1,x_2) + x_3 a_3(x_1,x_2) \tag{7}$$

for all $(x_1,x_2,x_3) \in \bar{\omega} \times [-\varepsilon, \varepsilon]$, where $\hat{\omega} = \theta(\bar{\omega})$ describes the parametrized middle surface and $\bar{\omega} \subset \mathbb{R}^2$. This is illustrated in Figure 3. Throughout the text greek indices take the values $1,2$ and latin indices take the values $1,2,3$. Let $\theta_{,\alpha}$ denote the partial derivatives of θ. At any point of $\bar{\omega}$, the two vectors

$$a_\alpha = \theta_{,\alpha} \quad \alpha \in \{1,2\} \tag{8}$$

span the tangent plane of the middle surface. The components of the first fundamental form (resp. the covariant metric tensor) are given by

$$a_{\alpha\beta} = a_\alpha \cdot a_\beta. \tag{9}$$

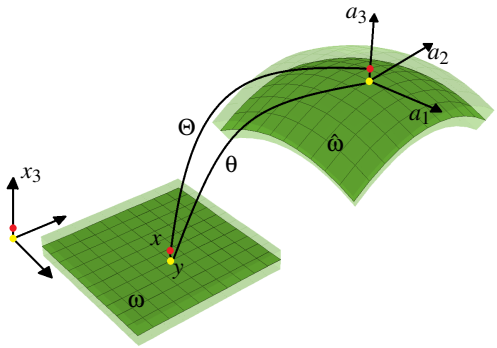

Figure 3: *Parametrization of the shell.*

The components $a^{\alpha\beta}$ of the contravariant metric tensor are defined by $a^{\alpha\gamma}a_{\gamma\beta} = \delta^{\alpha}_{\beta}$. The area element of $\hat{\omega}$ is $d\hat{\omega} = \sqrt{a}dx_1dx_2$, where $\sqrt{a} = |a_1 \times a_2|$. The normal of the middle surface, is given by

$$a_3 = \frac{a_1 \times a_2}{|a_1 \times a_2|} \tag{10}$$

and the thickness of the shell is measured in this direction. The components of the second fundamental form are

$$b_{\alpha\beta} = -a_{3,\beta} \cdot a_{\alpha}. \tag{11}$$

For later reference, we introduce the covariant basis vectors of the shell,

$$g_{\alpha} = \Theta_{,\alpha} = a_{\alpha} + x_3 a_{3,\alpha}, \quad g_3 = a_3, \tag{12}$$

and the corresponding components of the first fundamental form $g_{ij} = g_i \cdot g_j$, $i,j \in \{1,2,3\}$.

3.1. Deformation of the Shell

Koiter's shell model [Koi66, Koi70] is based on the Kirchhoff–Love assumptions [Kir52, Lov88]:

1. any normal line through a point of the middle surface remains a normal line through the same point of the middle surface after deformation, and
2. for every point of the shell, the distance to the middle surface remains constant during deformation.

Under these assumptions, the deformed shell can be parametrized as

$$\Theta^{\eta}(x_1,x_2,x_3) := \theta^{\eta}(x_1,x_2) + x_3 a_3^{\eta}(x_1,x_2), \tag{13}$$

where the deformed state of the middle surface is given by $\theta^{\eta}(x_1,x_2) := \theta(x_1,x_2) + \eta$, with the displacement vector field $\eta : \omega \to R^3$. The vector a_3^{η} describes the normal vector of the deformed middle surface. The difference between the metric tensors of the undeformed and deformed state of the shell is measured by the Green–Lagrange strain tensor:

$$\varepsilon_{ij} = \frac{1}{2}\left(g_{ij}^{\eta} - g_{ij}\right) \tag{14}$$

where g_{ij}^{η} denotes the covariant metric tensor of the deformed shell. The strain tensor can be written in terms of the first and second fundamental form of the undeformed and the deformed middle surface. Here, we consider a linearization of this tensor, which is given by

$$\varepsilon_{\alpha\beta} = \gamma_{\alpha\beta} + x_3\rho_{\alpha\beta}, \tag{15}$$

where $\alpha,\beta \in \{1,2\}$. The tensors γ and ρ are the linearized metric strain tensor and the linearized bending strain tensor; their components are given by

$$\gamma_{\alpha\beta} = \tfrac{1}{2}\left[a_{\alpha\beta}^{\eta} - a_{\alpha\beta}\right]^{lin} = \tfrac{1}{2}\left(a_{\alpha}\cdot\eta_{,\beta} + \eta_{,\alpha}\cdot a_{\beta}\right) \tag{16}$$

and

$$\begin{aligned}\rho_{\alpha\beta} &= \left[b_{\alpha\beta}^{\eta} - b_{\alpha\beta}\right]^{lin} \\ &= -\eta_{,\alpha\beta} + \frac{1}{2}\left(\eta_{,1}\cdot\left(a_{\alpha,\beta}\times a_2\right) + \eta_{,2}\cdot\left(a_1\times a_{\alpha,\beta}\right)\right) \\ &\quad + \frac{1}{\sqrt{a}}\left(a_3\cdot a_{\alpha,\beta}\right)\left(\eta_{,1}\cdot\left(a_2\times a_3\right) + \eta_{,2}\cdot\left(a_3\times a_1\right)\right).\end{aligned} \tag{17}$$

We consider two types of external forces: surface forces f acting on the middle surface $\hat{\omega}$ and boundary forces h acting on the boundary of the middle surface $\hat{\varphi} = \partial\hat{\omega}$. Then, the (linearized) thin shell model describes deformations of an elastic thin shell by a minimization problem: the unknown displacement vector field η should be the minimizer of the quadratic functional

$$\begin{aligned}j(\eta) &= \frac{2E}{1-\nu^2}\int_{\hat{\omega}} H^{\alpha\beta\sigma\tau}\left(\varepsilon\gamma_{\sigma\tau}\gamma_{\alpha\beta} + \frac{\varepsilon^3}{3}\rho_{\sigma\tau}\rho_{\alpha\beta}\right)\mathrm{d}\hat{\omega} \\ &\quad - \int_{\hat{\omega}} f\cdot\eta\,\mathrm{d}\hat{\omega} - \int_{\hat{\varphi}} h\cdot\eta\,\mathrm{d}\hat{\varphi},\end{aligned} \tag{18}$$

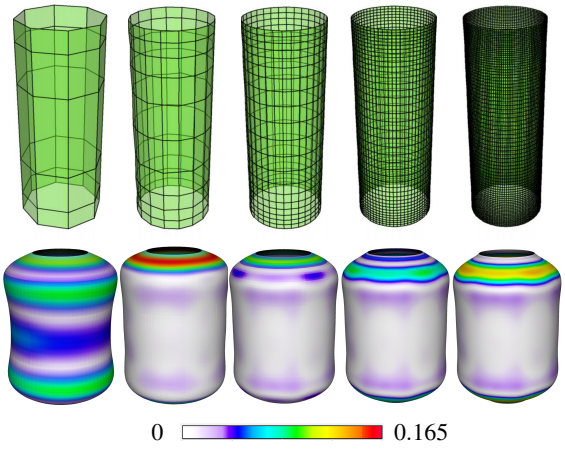

Figure 4: *Control grids 1-5 of the cylindrical shell and limit surfaces of the deformed states of this control grids. The color coding of the surfaces corresponds to the deviation of the numerical solution from the exact solution.*

over an appropriate set of vector fields η. Here, E and ν are material constants: the Young modulus and the Poisson ratio. The tensor

$$H^{\alpha\beta\sigma\tau} = \nu a^{\alpha\beta} a^{\sigma\tau} + \frac{1}{2}(1-\nu)\left(a^{\alpha\sigma}a^{\beta\tau} + a^{\alpha\tau}a^{\beta\sigma}\right). \quad (19)$$

is the shell elasticity tensor. We refer to [Cia05] for a derivation of the thin shell energy.

4. Discretization with a Catmull–Clark Finite Element

To obtain a conforming discretization of the thin shell energy, the finite element space we use needs to be a subspace of the Sobolev space H^2. Limit surfaces of Catmull–Clark's subdivision scheme are H^2-regular. This motivates us to use a finite element space constructed from limit surfaces of Catmull–Clark's subdivision scheme. This section splits in two parts: first, we describe a general scheme for the discretization of Koiter's thin shells, which is independent of the choice of a particular finite element space; and, second, we discuss how a finite element space that is based on Catmull–Clark's subdivision scheme can be used in this setting.

4.1. Discretization of the Shell Energy

The general form of the discretization of the shell energy, we discuss in this section, follows the approach introduced by Cirac at al. [COS00]. Because of the strain tensors (16) and (17) are symmetric, they can be represented in Voigt's notation

$$\gamma = \begin{pmatrix} \gamma_{11} \\ \gamma_{22} \\ \gamma_{12} \end{pmatrix}, \quad \rho = \begin{pmatrix} \rho_{11} \\ \rho_{22} \\ \rho_{12} \end{pmatrix}.$$

Again using Voigt notation, the elastic tensor (19), can be represented by the matrix:

$$H = \begin{pmatrix} a^{11}a^{11} & h_1 & a^{11}a^{12} \\ & a^{22}a^{22} & a^{22}a^{12} \\ sym. & & h_2 \end{pmatrix}, \quad (20)$$

where

$$\begin{aligned} h_1 &= \nu a^{11}a^{22} + (1+\nu)a^{12}a^{12}, \\ h_2 &= \frac{1}{2}\left((1-\nu)a^{11}a^{22} + (1+\nu)a^{12}a^{12}\right). \end{aligned}$$

In the discrete setting, we consider a mesh that partitions the domain ω. The set $\omega_h = \{\omega_i | i = 1, \ldots, noe\}$ describes the partition elements, where ω_i denotes the domain of the ith element, *noe* is the number of the mesh elements, and *nov* is the number of vertices. To describe a finite element space on ω, we specify a set of *nov* functions N^i, the shape functions, that form a basis of the space. Then, a displacement of the shell is given by

$$\eta_h(x_1, x_2) = \sum_{i=0}^{nov} \eta_i N^i(x_1, x_2), \quad (21)$$

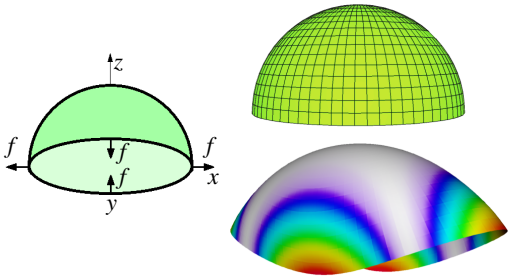

Figure 5: *Deformation of a hemisphere under the action of external forces. Equal and opposite concentrated forces are applied at antipodal points of the equator. Problem description, mesh and deformed state are presented. The coloring corresponds to the contours of displacement in direction of the load.*

where $\eta_i \in \mathbb{R}^3$. In the basis formed by the shape functions, the linearized metric and bending strains are represented by matrices M^i and B^i that satisfy

$$\gamma_h = \sum_{i=1}^{nov} M^i \eta_i, \quad \text{and} \quad \rho_h = \sum_{i=1}^{nov} B^i \eta_i.$$

Explicit formula for these matrices are provided in the appendix.

The discrete counterpart of the functional j is a quadratic functional on the finite element space. To solve the discrete minimization problem we need to solve the system of linear equations

$$K_h \eta_h = f_h \quad (22)$$

where K_h is the shell stiffness matrix, f_h the force vector, and η_h the unknown displacement. The entry with indices ij of the matrix K_h is given by

$$\begin{aligned} K_h^{ij} &= \sum_{k=1}^{noe} \left(\frac{2\varepsilon E}{1-\nu^2} \int_{\hat{\omega}_k} \left(M^i\right)^T H M^j \mathrm{d}\hat{\omega}_k \right. \\ &\quad \left. + \frac{2\varepsilon E}{3(1-\nu^2)} \int_{\hat{\omega}_k} \left(B^i\right)^T H B^j \mathrm{d}\hat{\omega}_k \right) \quad (23) \\ &= \sum_{k=1}^{noe} K_k^{ij}. \end{aligned}$$

The force vector f_h has the entries

$$f_h^i = \sum_{k=1}^{noe} \left(\int_{\hat{\omega}_k} f \cdot N^i \mathrm{d}\hat{\omega}_k + \int_{\hat{\varphi}_k} h \cdot N^i \mathrm{d}\hat{\varphi}_k \right) = \sum_{k=1}^{noe} f_k^i. \quad (24)$$

The matrices K_k and the vectors f_k are called the local stiffness matrices and the local force vector.

4.2. A Catmull–Clark Finite Element

We consider a Catmull–Clark limit surface that describes the middle surface of an undeformed shell. The limit surface, in

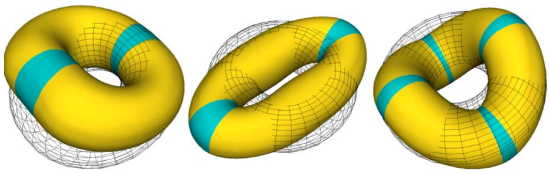

Figure 6: *Deformation-based modeling of a torus.*

turn, is specified by a control mesh. Any variation of the vertices of the control mesh induces a variation of the middle surface and consequently describes a deformation of the shell. We restrict the set of possible deformations of the shell to the set generated by all possible variations of the vertices of the control grid. This set forms a $(3\,nov)$-dimensional vector space. The displacement vector field η_h corresponding to a deformation of the shell has the form (21), where the shape functions N^i are evaluated as described in Section 2.2.

To set up the matrix K_h, we need to evaluate the integrals (23). The N^is have local support, therefore the sum over all elements in (23) reduces to a sum over the elements in the intersection of the supports of N^i and N^j. Since the intersection of the support of two shape functions is in most cases empty, the stiffness matrix K_h is a sparse matrix. To set up the matrix K_h, we iterate over all elements of the control mesh and for every element we compute the local matrix K_k and add it to the global matrix. The vertices of the control mesh that contribute to the local matrix K_k of an element are all the vertices that are in one of the stencils of the element, see Figure 2. For numerical evaluation of the integrals, we use the Gauß–Lagrange scheme, see [DHB02]. To set up the force vector f_h, we proceed analogously.

After setting up K_h and f_h, the displacement η_h of the control vertices is determined as the solutions of the linear system (22). To solve the system, we use a sparse factorization of the stiffness matrix. The deformation of the control grid is given by translation of the grid vertices from the undeformed to the deformed state along the calculated displacement field η_h. Finally, the deformed state of the middle surface described by the limit surface of the deformed control grid.

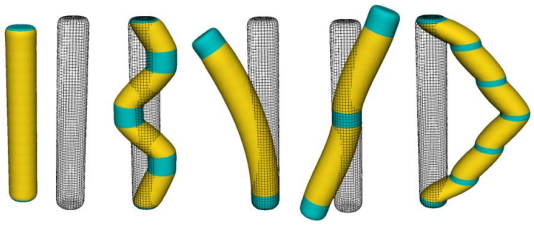

Figure 7: *Deformation-based modeling of a cylinder.*

5. Experiments

In this section, we present three applications of our discretization of Koiter's shells with Catmull–Clark finite elements: physical simulations, surface modeling, and modal analysis. Some of the meshes used in the experiments were generated with the QuadCover algorithm [KNP07]. For Section 5.2 and 5.3 the material constants of the shell are thickness $\varepsilon = 0.1$, Young's modulus $E = 1 \cdot 10^6$, and Poisson's ratio $\nu = 0.0$.

5.1. Physical Deformations

In the first example, we consider a thin cylindrical shell with fixed ends, which is affected by an uniform internal pressure that causes a deformation of the shell in normal direction. The exact solution of this problem was calculated by Timoshenko and Woinowsky–Krieger [TWK59]. The cylinder we consider has length 5, radius 1, and thickness 0.1 and its material constants are $E = 1 \cdot 10^5$ and $\nu = 0.0$. We simulate the deformation with 5 grids of increasing resolution, which we obtained by Catmull–Clark subdividing the coarsest grid. Results and control grids are shown in Figure 4. The color coding illustrates the deviation of the numerical solution from the exact solution and it can be seen that the finer grids produce more accurate results. The finest grid on the one hand produces a larger error than the previous grid in some areas, but on the other hand it approximates the boundary more accurately.

In a second experiment, we examine a pinched hemisphere with a fixed pole that is affected by force acting at four points on the equator. The hemisphere has radius 1, thickness 0.01, and material constants $E = 1 \cdot 10^6$ and $\nu = 0,1$. The grid we use for the simulation has one irregular vertex that is located at the pole. The result is shown in Figure 5, where the color coding indicates the deviation of the deformed shell from the hemisphere.

5.2. Surface Modeling

For deformation-based editing of surfaces, a deformation energy is used to describe the elastic behavior of a surface to be modeled. A designer can edit a surface by specifying forces that act on the surface, the modeling system returns a static solution in which the forces specified by the user

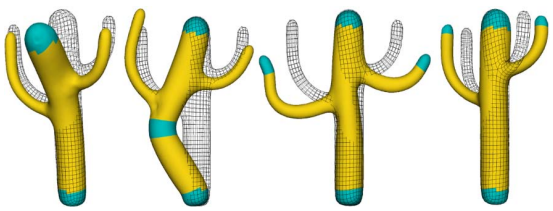

Figure 8: *Deformation-based modeling of a cactus model.*

and the forces of the surface that counteract a deformation are in an equilibrium. A benefit of such modeling systems is that they allow to describe complex editing operations with only few constraints. To be intuitive to use, the computed deformations need to be physically meaningful. We use our discretization of thin shells to compute such deformations. For a background on deformation-based modeling, we refer to [BS08].

In our modeling system the designer marks parts of the surface as handles and applies a rigid motion to each of the handles. Then, the system computes forces that pull the handles towards the specified new positions. The forces act like springs with zero rest length, hence have a quadratic potential energy. Then the energy of the modeling system is the sum of the thin shell energy and potential energy of the forces that act on the handles. To compute a deformation, our modeling system needs to find a minimum of this energy. This means it needs to solve an unconstrained quadratic problem, which amount to solving a system of linear equations. Since the matrix of the linear system remains the same as long as the same handles are used, it is efficient to compute a sparse factorization of the matrix and to use it to solve all the systems. This strategy allows for interactive modeling of the surface.

Surface deformations computed with our system are shown in Figure 6, 7 and 8. The handles are colored blue and the flexible parts of the surface are yellow. The control grids of undeformed surfaces are shown as well.

5.3. Vibration Modes

As a third application, we compute free vibration modes of thin shells. The modes are given as the solutions of the generalized eigenvalue problem

$$K_h \phi_h = \lambda M_h \phi_h, \tag{25}$$

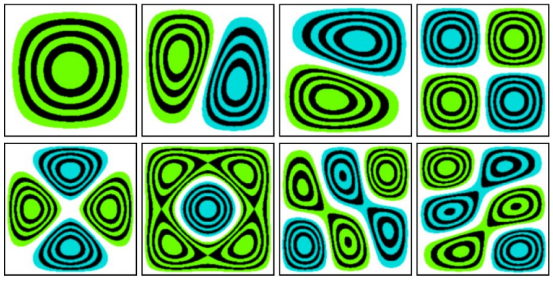

Figure 9: *Eight first modes of the Laplacian. The coloring corresponds to the contours of the displacement: the changes in positive z-direction are shown as green-black areas, in negative z-direction as blue-black area respectively.*

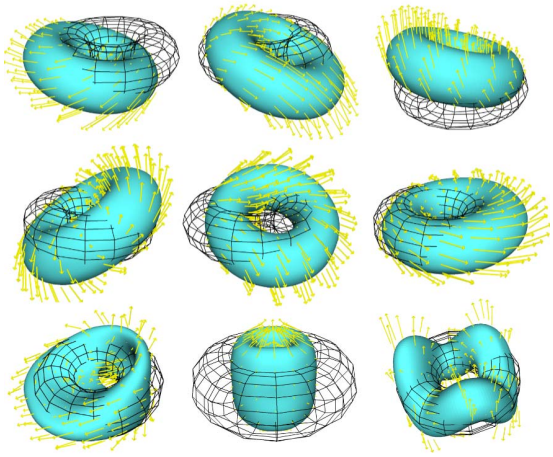

Figure 10: *Different vibration modes of the torus. For comparison, the initial grid is pictured. Additionally to the limit surface, the vector field of the corresponding mode is represented.*

where K_h is the stiffness matrix (see (23)), M_h the mass matrix, ϕ_h a vibration mode, and $\sqrt{\lambda}$ the corresponding eigenfrequency. We refer to [HSvTP10] for details.

To simplify the computation we have used a diagonal mass matrix instead of the full mass matrix in our experiments. The ith diagonal entry of this matrix equals a quarter of the sum of the surface areas of the elements adjacent to the ith vertex of the grid. The resulting generalized eigenvalue problem can be transferred into a standard eigenvalue problem using the technique discussed in [VL08]. We use a Jacobi procedure to solve the standard eigenvalue problem.

Resulting vibration modes are shown in Figures 9, 10, and 11. The first example shows modes of a clamped plate, the second shows eigenmodes of the torus (where the first six are the linearized rigid body motions), and the third example shows eigenmodes of a double torus.

References

[BHU10] BURKHART D., HAMANN B., UMLAUF G.: Isogeometric Finite Element Analysis Based on Catmull–Clark Subdivision Solids. *Computer Graphics Forum 29*, 5 (2010), 1575–1584. 2

[BPGK06] BOTSCH M., PAULY M., GROSS M., KOBBELT L.: PriMo: Coupled Prisms for Intuitive Surface Modeling. In *Eurographics Symposium on Geometry Processing* (2006). 1

[BS08] BOTSCH M., SORKINE O.: On Linear Variational Surface Deformation Methods. *IEEE Transactions on Visualization and Computer Graphics 14* (2008), 213–230. 1, 7

[CC78] CATMULL E., CLARK J.: Recursively Generated B-spline Surfaces on Arbitrary Topological Meshes. *Computer Aided Geometric Design 10* (1978), 350–355. 1, 2

[Cia05] CIARLET P.: *An Introduction to Differential Geometry with Applications to Elasticity*. Springer, Dordrecht, 2005. 5

[CO01] CIRAK F., ORTIZ M.: Fully C^1-conforming Subdivision Elements for Finite Deformation Thin-Shell Analysis. *International Journal for Numerical Methods in Engineering 51*, 7 (2001), 813–833. 2

[COS00] CIRAK F., ORTIZ M., SCHRÖDER P.: Subdivision Surfaces: A New Paradigm for Thin-Shell Finite-Element Analysis. *International Journal for Numerical Methods in Engeneering 47* (2000), 2039–2072. 2, 5

[CSA*02] CIRAK F., SCOTT M. J., ANTONSSON E. K., ORTIZ M., SCHRÖDER P.: Integrated Modeling, Finite-Element Analysis, and Engineering Design for Thin-Shell Structures using Subdivision. *Computer-Aided Design 34* (2002), 137–148. 2

[DHB02] DEUFLHARD P., HOHMANN A., BORNEMANN F. A.: *Numerische Mathematik*, 3., überarb. und erw. aufl. ed. De-Gruyter-Lehrbuch. Av4 Gruyter, Berlin, New York, 2002. 6

[HCY05] HUGHES T., COTTRELL J., Y. B.: Isogeometric Analysis: CAD, Finite Elements, NURBS, Exact Geometry and Mesh Refinement. *Computer Methods in Applied Mechanics and Engineering 194*, 39-41 (2005), 4135 – 4195. 1

[HSvTP10] HILDEBRANDT K., SCHULZ C., VON TYCOWICZ C., POLTHIER K.: Eigenmodes of Surface Energies for Shape Analysis. In *Advances in Geometric Modeling and Processing* (2010), vol. 6130 of *Lecture Notes in Computer Science*, Springer, pp. 296–314. 7

[Kir52] KIRCHHOFF G.: Über die Gleichungen des Gleichgewichtes eines elastischen Körpers bei nicht unendlich kleinen Verschiebungen der Theile. *Sitzungsberichte der mathem.-naturw. Classe der kais. Akademie der Wissenschaften 9* (1852), 762–773. 2, 4

[KNP07] KÄLBERER F., NIESER M., POLTHIER K.: QuadCover - Surface Parameterization using Branched Coverings. *Computer Graphics Forum 26*, 3 (2007), 375–384. 6

[Koi66] KOITER W.: On the Nonlinear Theory of Thin Elastic Shells. *Proc. Konik. Ned. Akad. Wetensch. 69* (1966), 1–54. 2, 4

[Koi70] KOITER W.: On the Foundations of the Linear Theory of Thin Elastic Shells. *Proc. Konik. Ned. Akad. Wetensch. 73* (1970), 169–195. 2, 4

[Lov88] LOVE A.: The Small Free Vibrations and Deformations of a Thin Elastic Shell. *Philosophical Transactions of the Roal Society Ser. A 179* (1888), 491–549. 2, 4

[Ma05] MA W.: Subdivision Surfaces for CAD - an Overview. *Computer Aided Design 37* (2005), 693–709. 2

[PEK*08] PETERS J., EDELSBRUNNER H., KOBBELT L., POLTHIER K., REIF U.: *Subdivision Surfaces*. Geometry and Computing. Springer, Berlin, Heidelberg, 2008. 2

[RS01] REIF U., SCHRÖDER P.: Curvature Integrability of Subdivision Surfaces. *Advances in Computational Matkematics 14* (2001), 157–174. 2

[Sta98] STAM J.: Exact Evaluation of Catmull–Clark Subdivision Surfaces at Arbitrary Parameter Values. In *SIGGRAPH 98 Conference Proceedings, Annual Conference Series* (New York, NY, USA, 1998), ACM, pp. 395–404. 2, 3

[TWK59] TIMOSHENKO S., WOINOWSKY-KRIEGER S.: *Theory of Plates and Shells*. McGraw–Hill, New York, 1959. 6

[VL08] VALLET B., LÉVY B.: Spectral Geometry Processing with Manifold Harmonics. *Computer Graphics Forum 27*, 2 (2008), 251–260. 7

Appendix

In this appendix, we describe the coefficients of membrane and bending strain matrices introduced in Section 4.1. Let

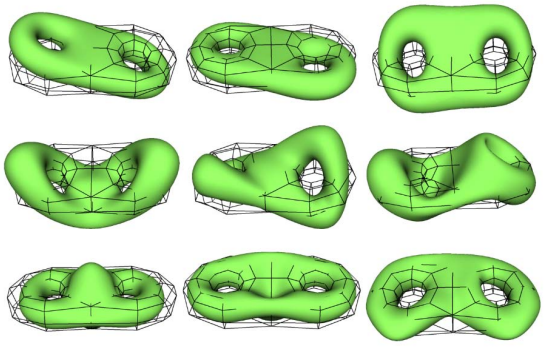

Figure 11: *Different vibration modes of a double torus.*

(e_1, e_2, e_3) denote the standard basis of $\mathbb{R}^3$. Then, the membrane and bending strain matrices take the form:

$$M^i = \begin{pmatrix} M^i_1 \cdot e_1 & M^i_1 \cdot e_2 & M^i_1 \cdot e_3 \\ M^i_2 \cdot e_1 & M^i_2 \cdot e_2 & M^i_2 \cdot e_3 \\ M^i_3 \cdot e_1 & M^i_3 \cdot e_2 & M^i_3 \cdot e_3 \end{pmatrix}$$

with

$$\begin{aligned} M^i_1 &= N^i_{,1} a_1, \\ M^i_2 &= N^i_{,2} a_2, \\ M^i_3 &= \left(N^i_{,2} a_1 + N^i_{,1} a_2\right), \end{aligned}$$

and

$$B^i = \begin{pmatrix} B^i_1 \cdot e_1 & B^i_1 \cdot e_2 & B^i_1 \cdot e_3 \\ B^i_2 \cdot e_1 & B^i_2 \cdot e_2 & B^i_2 \cdot e_3 \\ 2B^i_3 \cdot e_1 & 2B^i_3 \cdot e_2 & 2B^i_3 \cdot e_3 \end{pmatrix},$$

where

$$\begin{aligned} B^i_1 = -N^i_{,11} a_3 \quad &+ \quad \tfrac{1}{\sqrt{a}} \left[N^i_{,1} a_{1,1} \times a_2 + N^i_{,2} a_1 \times a_{1,1} \right. \\ &+ \quad \left. a_3 \cdot a_{1,1} \left(N^i_{,1} a_2 \times a_3 + N^i_{,2} a_3 \times a_1 \right) \right] \end{aligned}$$

$$\begin{aligned} B^i_2 = -N^i_{,22} a_3 \quad &+ \quad \tfrac{1}{\sqrt{a}} \left[N^i_{,1} a_{2,2} \times a_2 + N^i_{,2} a_1 \times a_{2,2} \right. \\ &+ \quad \left. a_3 \cdot a_{2,2} \left(N^i_{,1} a_2 \times a_3 + N^i_{,2} a_3 \times a_1 \right) \right] \end{aligned}$$

$$\begin{aligned} B^i_3 = -N^i_{,12} a_3 \quad &+ \quad \tfrac{1}{\sqrt{a}} \left[N^i_{,1} a_{1,2} \times a_2 + N^i_{,2} a_1 \times a_{1,2} \right. \\ &+ \quad \left. a_3 \cdot a_{1,2} \left(N^i_{,1} a_2 \times a_3 + N^i_{,2} a_3 \times a_1 \right) \right]. \end{aligned}$$